Towards an assessment of riverine dissolved organic carbon in surface waters of the Western Arctic Ocean based on remote sensing and biogeochemical modeling

[1]Vincent Le Fouest

[2,3]Atsushi Matsuoka

[4]Manfredi Manizza

[1]Mona Shernetsky

[5]Bruno Tremblay

[2,3]Marcel Babin

[1]Littoral Environnement et Sociétés, UMR 7266, Université de La Rochelle, La Rochelle, France

[2]Takuvik Joint International Laboratory, Université Laval & CNRS, Québec, QC, G1V 0A6, Canada

[3]Takuvik Joint International Laboratory, CNRS, Québec, QC, G1V 0A6, Canada

[4]Geosciences Research Division, Scripps Institution of Oceanography, University of California San Diego, La Jolla, CA 92093-0244, USA

[5]Department of Atmospheric and Oceanic Sciences, McGill University, Montreal, QC, H3A OB9, Canada

Abstract

Future climate warming of the Arctic could potentially enhance the load of terrigenous dissolved organic carbon (tDOC) of Arctic rivers due to increased carbon mobilization within watersheds. A greater flux of tDOC might impact the biogeochemical processes of the coastal Arctic Ocean (AO) and ultimately its capacity of absorbing atmospheric CO_2. In this study, we show that sea surface tDOC concentrations simulated by a physical-biogeochemical coupled model in the Canadian Beaufort Sea for 2003-2011 compare favorably with estimates retrieved by satellite imagery. Our results suggest that, over spring-summer, tDOC of riverine origin contributes to 35 % of primary production and that an equivalent of ~10 % of tDOC is exported westwards with the potential for fueling the biological production of the eastern Alaskan nearshore waters. The combination of model and satellite data provide promising results to extend this work to the entire AO so as to quantify, in conjunction with in-situ data, the expected changes in tDOC fluxes and their potential impact on the AO biogeochemistry at basin scale.

1. Introduction

The Arctic Ocean (AO) receives ~10% of the global freshwater discharge (Opsahl et al., 1999 and references therein), of which the larger part (~54-64 %) originates from six main pan-Arctic rivers (Haine et al., 2015; Holmes et al., 2012; Aagaard and Carmack, 1989). Over the past 30 years, the Arctic freshwater cycle intensified as reflected by changes in snow cover (Bring et al., 2016), evapotranspiration from terrestrial vegetation (Bring et al., 2016), and precipitation (Vihma et al., 2016). It resulted in an increase of the freshwater discharge from North American and Eurasian rivers by ~2.6 % and ~3.1 % per decade, respectively (Holmes et al., 2015). More than half the soil organic carbon stock on Earth is contained in the permafrost of the Arctic watersheds (Tarnocai et al., 2009). With the warming of the lower atmosphere, the permafrost undergoes a substantial thawing (Romanovsky et al., 2010) likely to alter the organic carbon content and quality of inland waters. In the past decades, the flux of dissolved organic carbon (DOC) decreased in the Yukon River (40 %; Striegl et al., 2005) while it increased at the Mackenzie River mouth (~39 %; Tank et al., 2016). These contrasting responses to climate change suggest that the direction of future trends of DOC concentrations and fluxes to the AO are very uncertain (Abbott et al., 2016).

The coastal AO influenced by large river plumes is hence exposed to changing conditions. Coastal waters are supplied in riverine organic carbon all year round with a maximal flux in spring-early summer when the freshwater discharge reaches a seasonal maximum. In river waters, DOC is present in higher concentration than the particulate form (Le Fouest et al., 2013; Dittmar et al., 2003). It accounts for more ~82 % of the flux of total riverine organic carbon (McGuire et al., 2009). The pan-Arctic flux of riverine DOC to the AO is estimated to be 33-37.7 TgC yr^{-1} (Holmes et al., 2012; Manizza et al., 2009; McGuire et al., 2009; Raymond et al., 2007). As the organic carbon formed by phytoplankton, terrigenous DOC (tDOC) can be considered new carbon fueling annually the upper AO. In that respect, and regardless of its distinct nature and fate, the flux of riverine DOC would be equivalent to 10-19 % of AO primary production (Stein and Macdonald, 2004; Bélanger et al., 2013). In the oligotrophic Beaufort Sea, this proportion would reach ~34 % (S. Bélanger, pers.

64 comm.). Riverine DOC is hence a significant pool in the Arctic carbon cycle that can markedly
65 modify the biological production and biogeochemistry of the AO waters. Within the pelagic food
66 web, riverine DOC can be assimilated and transformed, promoting both phytoplankton and
67 bacterioplankton production (Le Fouest et al., 2015; Tank et al., 2012). Riverine DOC can also
68 modulate the air-sea fluxes of CO_2. In present climatic conditions, Manizza et al. (2011) suggest
69 that the mineralization of riverine DOC into dissolved inorganic carbon would induce a 10 %
70 decrease of the net oceanic CO_2 uptake at the pan-Arctic scale. On East Siberian shelves, the
71 degradation of terrestrial organic carbon would be partly responsible for sea surface acidification
72 (Semiletov et al., 2016).
73 In recent studies, riverine DOC flux data were used in a 3D ocean-biogeochemical coupled model
74 to investigate the fate of riverine DOC within surface Arctic waters (Le Fouest et al., 2015; Manizza
75 et al., 2013, 2011, 2009). However, simulated spatial and temporal changes in riverine DOC
76 concentrations have not yet been compared with remote sensing data to assess the model predictive
77 ability. Such a model-satellite comparison allows validating the model and then using it with
78 confidence to resolve the annual cycle of riverine DOC, a prerequisite for a robust assessment of the
79 riverine DOC contribution to the Arctic carbon cycle. To this end, riverine DOC concentrations at
80 the sea surface obtained from a previous model run described in Le Fouest et al. (2015) and tDOC
81 concentrations derived from remote sensing data were analyzed for the Canadian Beaufort Sea. As
82 riverine DOC accounts for more than 99 % of the total tDOC exported to the AO (McGuire et al.,
83 2009), we will use the term tDOC for both the model and remotely sensed data. Our goals are to
84 compare tDOC data derived from the model and from remote sensing using skill metrics, in order to
85 assess the model capacity to reproduce the observed seasonal and spatial variability in tDOC, and to
86 provide bulk estimates of the seasonal tDOC stock and lateral fluxes within the surface coastal
87 waters using a combination of these two approaches.
88 The paper is organized as follows. First, we describe the two different approaches used to quantify
89 tDOC within the AO, i.e. a semi-analytical method based on remote sensing and a regional ocean-

biogeochemical coupled model that includes explicit fluxes of riverine DOC to the AO. Second, we compare the distribution and export flux of tDOC within surface waters of the Beaufort Sea estimated by the model and remote sensing. Finally, we discuss future developments of biogeochemical models necessary to simulate successfully the carbon budget of Arctic coastal waters in a warming world.

2. Material and methods

2.1 Remote sensing data

Level 1A scene images acquired from the MODerate-resolution Imaging Spectroradiometer (MODIS) aboard the Aqua satellite were downloaded from the NASA ocean color website (https://oceandata.sci.gsfc.nasa.gov/MODIS-Aqua/L1/). After geometric correction, remote sensing reflectance, Rrs(λ) data at 412, 443, 488, 531, 555, and 667 nm were obtained by applying the atmospheric correction proposed by Wang and Shi (2009) with modifications adapted to Arctic environments (Doxaran et al., 2015; Matsuoka et al., 2016). The light absorption coefficients of colored dissolved organic matter at 443 nm ($a_{CDOM}(443)$) were derived from the Rrs(λ) data using the gsmA algorithm (Matsuoka et al., 2017) that optimizes the difference between satellite Rrs(λ) and Rrs(λ) calculated using parameterization of absorption and backscattering coefficients for Arctic waters (Matsuoka et al., 2011, 2013). tDOC concentrations were estimated from the $a_{CDOM}(443)$ data using an empirical relationship between DOC and $a_{CDOM}(443)$ established in the Southern Beaufort Sea (Matsuoka et al., 2013). Since DOC concentrations estimated using ocean color data are based on a highly significant DOC versus $a_{CDOM}(443)$ relationship (R^2 = 0.97; Matsuoka et al., 2012), the DOC is considered to be of terrestrial origin. Errors of intercept, slope, and $a_{CDOM}(443)$ were propagated into the in-situ (empirical) DOC versus $a_{CDOM}(443)$ relationship. It resulted into a mean uncertainty of the tDOC concentration estimates of 28 % (see Appendix A2 of Matsuoka et al., 2017). Scene images of tDOC concentrations were used to make monthly

115 composite images at 1 km horizontal resolution of the Mackenzie shelf in the Canadian Beaufort
116 Sea (Fig. 1).
117
118 **2.2 3D physical-biogeochemical model data**
119 We used sea surface tDOC concentrations and ocean currents simulated over 2003-2011 by a
120 previous pan-Arctic model run ("RIV run") whose setup is fully detailed in Le Fouest et al. (2015).
121 The pan-Arctic model data were extracted on the remote sensing geographical domain focused on
122 the southern Beaufort Sea. We provide here a brief description of the physical-biogeochemical
123 coupled model used to generate the "RIV run". The MITgcm (MIT general circulation model)
124 ocean-sea ice model (Nguyen et al., 2011, 2009; Losch et al., 2010; Condron et al., 2009) has a
125 variable horizontal resolution of ~18 km and covers the Arctic domain with open boundaries at
126 55°N on the Atlantic Ocean and Pacific Ocean sides. The open ocean boundaries are constrained by
127 potential temperature, salinity, flow, and sea-surface elevation derived from integrations of a global
128 configuration of the MITgcm model (Menemenlis et al., 2005). Atmospheric forcings (10 m winds,
129 2 m air temperature and humidity, and downward long and short-wave radiation) are taken from the
130 six-hourly data sets of the Japanese 25 year ReAnalysis (JRA-25) (Onogi et al., 2007). In addition
131 to precipitations, the hydrologic forcing includes a monthly climatology of freshwater discharge
132 from 10 pan-arctic watersheds (Manizza et al., 2009). Monthly mean estuarine fluxes of freshwater
133 are based on an Arctic Runoff database (Lammers et al., 2001; Shiklomanov et al., 2000). For each
134 watershed, the river discharge forcing is associated with a monthly climatology of riverine DOC
135 concentration (Manizza et al., 2009). The total annual load of tDOC in the model is 37.7 TgC yr^{-1}. It
136 is consistent with previous values reported in Raymond et al. (36 TgC yr^{-1}; 2007) and Holmes et al.
137 (34 TgC yr^{-1}; 2012) and obtained by using load estimation models linking riverine DOC
138 concentrations to river discharge data. The physical model is coupled with a 10-compartment
139 biogeochemical model (Lee et al., 2016; Le Fouest et al, 2015). The biogeochemical model
140 explicitly accounts for dissolved inorganic nutrients (nitrate and ammonium), small and large

phytoplankton, protozooplankton, mesozooplankton, bacterioplankton, detrital particulate and dissolved organic nitrogen, and tDOC (Lee et al., 2016; Le Fouest et al., 2015). The tDOC compartment couples the marine and terrestrial cycling of organic matter though tDOC recycling into inorganic nutrients by bacterioplankton. We set to 15 % the percentage of tDOC entering the model as usable by the bacterioplankton compartment. This value was estimated based on the mean yearly percentages of the total load of riverine DOC considered as biodegradable DOC for six major Arctic rivers given in Wickland et al. (2012).

2.3 Analysis

Remotely sensed and simulated tDOC data were binned for the months of June, July, August and September over the 9-year period (2003-2011) to get the best areal coverage in the satellite composites. The remotely sensed tDOC concentrations were regridded on the model horizontal grid. Skill metrics were used to compare the remotely sensed estimates of tDOC with their simulated counterparts. The metrics included the correlation coefficient (r), the unbiased root mean square error (RMSE), the Nash-Sutcliffe model efficiency index (MEF), the geometric bias, and the geometric RMSE (see Stow et al., 2009; Doney et al., 2009; Nash and Sutcliffe, 1970). The metrics are computed as follows:

$$r = \frac{\sum_{n=1}^{N}(sat_n -)\left(mod_n - \overline{mod}\right)}{\sqrt{\sum_{n=1}^{N}(sat_n - \overline{sat})^2 \sum_{n=1}^{N} mod_n - \overline{mod}^2}} \qquad (Eq.1)$$

$$unbiased\ RMSE = \sqrt{\frac{1}{N}\sum_{n=1}^{N}\left(mod_n - sat_n - \left(\overline{mod} - \overline{sat}\right)\right)^2} \qquad (Eq.2)$$

$$MEF = \frac{\sum_{n=1}^{N}(sat_n - \overline{sat})^2 - \sum_{n=1}^{N}(sat_n - mod_n)^2}{\sum_{n=1}^{N}(sat_n - \overline{sat})^2} \qquad (Eq.3)$$

$$geometric\ bias = e^{(\overline{mod} - \overline{sat})} \qquad (Eq.4)$$

$$geometric\ RMSE = \sqrt{e^{\left(\frac{1}{N}\sum_{n=1}^{N}(mod_n - sat_n)^2\right)}} \qquad (Eq.5)$$

where N is the number of tDOC data, and $\overline{sat}$ and $\overline{mod}$ are the remotely sensed and the simulated tDOC averages, respectively. Monthly fluxes of tDOC were calculated and summed along two cross-shelf transects (see upper-middle panel in Fig. 2). At each grid cell, the model flux estimate was computed as the product of the simulated sea surface current velocity with the simulated tDOC concentration. The remote sensing flux estimate was computed as the product of the simulated sea surface current velocity with the remotely sensed tDOC concentration.

3. Results and discussion

3.1 tDOC concentrations and distribution

Over the Mackenzie shelf, the plume of high-tDOC (> 120 mmolC m^{-3}) had a maximal areal extent in June for both the model and the satellite data (Fig. 2). This coincided with the seasonal peak of river discharge in June as parameterized in the model and generally depicted by in-situ time series (Yang et al., 2015). From July to September, the high-tDOC areal extent progressively decreased following the seasonal pattern of riverine freshwater discharge (see Yang et al., 2015; Manizza et al., 2009). This seasonal pattern was observed both in the model and satellite data. The simulated tDOC concentrations were lower than in the satellite record in Mackenzie Bay and east of the Mackenzie Bay, especially in June (by 44 % in average) and July (by 27 % in average). In the Beaufort and Chukchi seas, first year sea ice represents a carbon flux to the ocean of 2×10^{-4} TgC yr^{-1} (Rachold et al., 2004). This flux is 4 orders of magnitude lower than the tDOC supply from the Mackenzie River specified as boundary conditions in the model (2.54 TgC yr^{-1}). Similarly, tDOC eroded from permafrost stored in the North American shores would account for only ~0.5-1.6 $\times 10^{-4}$ TgC yr^{-1} (Tanski et al., 2016; Ping et al., 2011, using a DOC:POC ratio of 1:900 as in Tanski et al., 2016) to ~2×10^{-3} TgC yr^{-1} (McGuire et al., 2009). With regard to these flux values, tDOC originating from

183 both melted sea ice and eroded permafrost, not taken into account in the model, are hence not
184 believed to explain the model-satellite discrepancies (Fig. 2). Other factors might contribute to these
185 model-satellite differences observed nearshore. First, the model does not distinguish between the
186 two main pathways of the Mackenzie River discharge entering the shallow delta zone. In June, the
187 Mackenzie Bay receives most of the fresh and turbid river water (~66 %) while the remaining ~33 %
188 spreads east of the delta in Kugmallit Bay (Davies, 1975). This pattern was particularly well
189 captured by the remotely sensed data in June-July (Fig. 2). Second, the inner Mackenzie shelf (< 20
190 m depth) is bounded during winter by a thick ridged ice barrier grounded on the sea floor called
191 stamukhi (Macdonald et al., 1995). The stamukhi retains the turbid river water within the inner shelf
192 in winter. When sea ice breaks up and the freshet reaches its seasonal maximum in spring, the
193 retained turbid waters spread farther within the coastal zone. Contrary to the model, the remote
194 sensing data could resolve this particular feature explaining the higher tDOC concentrations
195 observed nearshore in June (see Fig. 2). Such a pattern observed for tDOC is also reported for
196 terrigenous particulate organic matter (Doxaran et al., 2015). Further offshore on the Mackenzie
197 shelf, as delimited by the 300 m isobaths both remotely sensed and simulated concentrations of
198 tDOC were within the range of values measured in spring (~110-230 mmolC m^{-3}; Osburn et al.,
199 2009) and summer (~60-100 mmolC m^{-3}; Para et al., 2014). The simulated values of tDOC were
200 higher than those remotely sensed on the outer and off the shelf. Overall, the model and the satellite
201 data captured the seasonal cycle and spatial distribution of tDOC concentrations in the study area.

202 Skill metrics were computed over the whole study area (see Fig. 2) to provide a quantitative
203 comparison of tDOC simulated with the model and satellite data (Table 1). For all months, the
204 correlation coefficient was relatively high ($0.78<r<0.82$) within the range of values obtained for sea
205 surface dissolved inorganic nutrients simulated by global models ($r>0.75$; Doney et al., 2009).
206 Regardless of amplitude, the r values showed that the simulated and remotely sensed tDOC
207 concentrations presented similar patterns of variation. The size of the model-satellite discrepancies
208 was given by the unbiased RMSE. Overall, the unbiased RMSE decreased from June (41.4 mmolC

209 m^{-3}) to September (29.3 mmolC m^{-3}). This result suggested that the model accuracy increased from
210 spring to summer. The model capability for predicting tDOC relative to the average of the remote
211 sensing counterparts was estimated by the model efficiency index ($-\infty < MEF \leq 1$) (Nash and
212 Sutcliffe, 1970). The MEF is a normalized statistic that relates the residual variance between the
213 simulated and remotely sensed tDOC concentrations to the variance within the remotely sensed
214 tDOC data (see Eq. 3). A MEF value near zero means that the residual variance compares to the
215 remotely sensed variance, i.e. that the model predictions are as accurate as the mean of the satellite
216 data. As the MEF increases towards a value of one, the residual variance becomes increasingly
217 lower than the observed variance. For all months, the MEF was positive (0.26-0.60) suggesting that
218 tDOC concentrations simulated by the model were an acceptable predictor relative to tDOC
219 concentrations derived from remote sensing, especially in June-July. In order to give a more even
220 weight to all of the data and to limit the skewness towards the higher tDOC concentrations, metrics
221 based on log-transformed tDOC data were also computed. For all months, the geometric RMSE was
222 close to one and range between 1.02 and 1.12. It suggested that the model-satellite data dispersion
223 was relatively small when the positive skewness was reduced. In June, the relatively high unbiased
224 RMSE could be partly due to high tDOC concentrations as suggested by the relatively low
225 geometric RMSE (1.07). Finally, the computed geometric bias informs with respect to the direction
226 of the model-satellite discrepancies. For all months, the geometric bias (1.07-1.32) was higher than
227 one meaning that the model tended, on average, to overestimate the observations over the whole
228 domain. The highest geometric bias was reported in August (1.32), when the river discharge was
229 low, suggesting that tDOC removal was likely underestimated in the model in late summer. A
230 Taylor diagram (Taylor, 2001) was produced to provide a synthetic and complementary overview of
231 how the simulated and remotely sensed tDOC concentrations compared seasonally in terms of
232 correlation, amplitude of variations (given by the standard deviations), and normalized model-
233 satellite discrepancies (Fig. 3). All months differed by their normalized RMSE and amplitude of
234 variations while the correlation coefficient was close to ~0.8 (see Table 1). The model best

235 performed in simulating tDOC in July, just after the seasonal peak of river discharge, followed by
236 the months of June and August. June and August showed similar values of correlation, RMSE, and
237 normalized standard deviation despite distinct seasonal patterns of river discharge (high and low,
238 respectively). By contrast, September showed the highest model-satellite data dispersion. With
239 respect to satellite estimates, the skill metrics overall suggested that the model could reliably
240 simulate tDOC concentrations in surface waters over a wide range of river discharge and tDOC load.

241

242 **3.2 tDOC stock and lateral export fluxes**

243 The overall agreement between the model and the satellite tDOC concentrations allowed the
244 assessment of the mean areal stock and lateral fluxes of tDOC using the mean surface ocean
245 circulation simulated by the MITgcm (Table 2). The monthly-averaged (June to September) areal
246 stock of tDOC over the Mackenzie shelf as delimited by the 300 m isobaths was estimated to 1.37
247 TgC (Table 2). The bias between the model and the satellite data was the highest in August but did
248 not exceed +8.2 % (0.1 Tg C). This result is consistent with the highest geometric bias reported in
249 August (Table 1). In the model, the removal of tDOC through photo-oxidation (Bélanger et al.,
250 2006) was not taken into account. Assuming an annual mean mineralization rate of tDOC of ~0.02
251 TgC (Bélanger et al., 2006), this process would explain <2 % of the reported tDOC difference in
252 August. In addition, the 15% value used to set the bioavailable tDOC fraction in the model was at
253 the low end of values reported in other studies (up to 50%; Mann et al., 2012; Wickland et al., 2012,
254 Letscher et al., 2011; Alling et al., 2010; Holmes et al., 2008). This underestimation of the
255 bioavailable fraction of tDOC upon delivery to the AO could be a major reason why the simulated
256 values of tDOC were consistently overestimated when compared to satellite estimates for the outer
257 shelf and offshore locations (Fig. 1, Table 1). In the model, bacterioplankton consumed tDOC to
258 produce ammonium usable in turn by phytoplankton. In the Beaufort Sea, this pathway contributed
259 to primary production by 35 % on average over 2003-2011. However, the simulated rates of
260 bacterioplankton production (< 30 mgC m^{-2} d^{-1}) still remained in the lower range of those measured

261 in the Beaufort Sea (25-68 mgC m^{-2} d^{-1}; Ortega-Retertua et al., 2012; Vallières et al., 2008). The
262 likely underestimation of the tDOC removal by bacterioplankton in the model during summer
263 months might largely contribute to the reported bias between the model and the satellite data.
264 Nevertheless, the bias remained moderate with respect to values reported for June, July and
265 September (-1.5 % to -2.8 %) (Table 2).

266 Combining the modeling and remote sensing approaches allowed for the reconstruction of the
267 dominant surface pattern in lateral tDOC fluxes in the Canadian Beaufort Sea from June to
268 September (Fig. 4). Two north-south transects were defined east (Cape Bathurst) and west
269 (Mackenzie Trough) of the Mackenzie shelf (see upper-middle panel in Fig. 2). The net seasonal
270 flux was westward along the two transects following the anticyclonic circulation pattern of the
271 Beaufort gyre (Mulligan et al., 2010) and was maximum in June and September. The flux was at
272 least three times higher along the western transect near the Mackenzie Through than east at Cape
273 Bathurst. This suggests a net export of tDOC towards the Alaskan part of the Beaufort Sea. In
274 contrast, whilst the flux in July and August remained oriented westward near the Mackenzie Trough,
275 it was reversed at Cape Bathurst. In July, the tDOC flux was still 1.3 to 1.7 times higher along the
276 western transect. In August, however, there was more tDOC (~1.4-fold) exported eastward at Cape
277 Bathurst than exported westward near the Mackenzie Through.

278 Along the two transects, the simulated fluxes were higher than those derived from remotely sensed
279 tDOC concentrations (Fig. 4). The monthly bias between the model and the satellite flux estimates
280 varied between 0 % and +18.2 %. The bias on the seasonal net flux was moderate (+8.3 %) near the
281 Mackenzie Trough but reached +25 % at Cape Bathurst. The seasonal mean flux however was one
282 order of magnitude lower than near the Mackenzie Trough. The flux estimates suggested that,
283 despite discrepancies in tDOC concentrations, the modeling and remote sensing approaches
284 provided robust estimates of the lateral transport of tDOC in surface waters in late spring-summer.
285 Because of sea ice and cloud cover, the satellite retrieval was limited to a temporal window
286 covering a third of a year only, i.e. from June to September. The yearly mean lateral flux of tDOC

287 was computed from the simulated data along the Mackenzie Trough transect and it reached 0.31
288 TgC. The flux of tDOC cumulated over June to September along this transect (0.12-0.13 TgC)
289 represented ~42 % of this annual flux (0.31 TgC), which is consistent with the fraction of the
290 annual discharge of freshwater by the Mackenzie that occurs during spring-summer (~50 %;
291 McClelland et al., 2012). Using stable isotope techniques on pelagic particulate organic matter, Bell
292 et al. (2016) showed that OC originating from the Mackenzie outflow in summer was incorporated
293 within bentho-pelagic food webs as far as the eastern Alaskan shelf. In nearshore waters of this part
294 of the Beaufort Sea, the study of Dunton et al. (2006) using stable isotopes also suggested that
295 tDOC from the Mackenzie River could add to the local terrigenous carbon inputs mediated by
296 coastal erosion and smaller rivers to fuel the biological production in summer. Using the model and
297 satellite data, we report that an equivalent of ~10 % (0.12-0.13 TgC) of the cumulated flux of tDOC
298 delivered by the Mackenzie River over spring-summer (1.32 TgC) was exported westward in the
299 Alaskan Beaufort Sea along the Mackenzie Trough transect.
300
301 **4. Perspectives**
302 The results of our study suggest that the model is in fair agreement with the surface tDOC fields
303 remotely sensed in spring-summer when most of the riverine flux occurs. The comparison allows an
304 evaluation of the model and justifies its use to resolve the annual cycle of tDOC. Because satellite
305 imagery provides data only during spring-summer, further uncertainties still remain in the model in
306 fall-winter in terms of tDOC concentrations and spatial distribution. In addition, the model involves
307 some limitations mostly due to the biogeochemical processing of tDOC. The tDOC transformation
308 is complex to translate into robust mechanistic equations as highly dependent on the availability of
309 in-situ data in Arctic waters. For instance, the riverine tDOC compartment is split in the model into
310 a labile and a non-labile fraction (see Le Fouest et al., 2015). This parameterization strongly
311 constrains the removal of tDOC by bacterioplankton and therefore the tDOC concentrations
312 simulated within surface waters. In natural waters, however, tDOC is made of a complex mixture of

compounds that differ by their chemical composition and age (Mann et al., 2016) and so along the seasons (Wickland et al., 2012, Mann et al., 2012). The chemical nature of tDOC impacts its bioavailability, which is estimated to average 6 % to 46 % of the total tDOC pool with marked disparities amongst the seasons and the rivers (Mann et al., 2012). Nevertheless, the general trend for the six major Arctic rivers (Kolyma, Yukon, Mackenzie, Ob, Yenisey and Lena) is a more labile tDOC pool in winter than in spring and summer (Wickland et al., 2012). In the Kolyma River, Mann et al. (2012) report a higher labile fraction in spring (~20 %) than in summer (<10 %) as the exported tDOC is younger during the freshet. Such a pattern is, however, not clearly present in the Mackenzie River (e.g. Wickland et al., 2012). We suggest that a more realistic representation in the model of the nature of the organic matter entering the coastal waters might improve the tDOC concentrations simulated in surface AO waters. It could include, for instance, the riverine flux of both dissolved organic carbon and nitrogen along with an improved C:N stoichiometry for bacterioplankton uptake (see Le Fouest et al., 2015).

In the model, the seasonal forcing of tDOC was based on DOC measurements gathered hundreds kilometers upstream the rivers' mouths. This precludes any DOC enrichment of the Mackenzie River water as it flows through the delta (see Emmerton et al., 2008) with, as a consequence, a likely underestimation of tDOC concentrations simulated in nearshore waters. Therefore, the quantification of the tDOC flux from the watersheds to the coastal AO poses as another key issue to addressing the role of tDOC in the biogeochemistry of shelf waters. Recently, watersheds models were developed to assess this tDOC flux (Tank et al., 2016; Kicklighter et al., 2013; Holmes et al., 2012). Such models provide realistic estimates but still require improvements as watersheds properties and mechanistic processes underlying the tDOC mobilization and riverine transport are complex to set up (see Kicklighter et al., 2013). The remote sensing of high resolution ocean color data is increasingly used to assess tDOC concentrations in large pan-Arctic rivers during the open water season (Herrault et al., 2016; Griffin et al., 2011). Ocean color techniques could then prove

338 useful in the future to improve the tDOC time series set at models boundaries by accounting for
339 instance for year-to-year variations of tDOC concentrations during the freshet period.
340 In our study, the remotely sensed tDOC concentrations retrieved in shelf waters provide the
341 advantage of already integrating the effect of the watersheds processes such as mobilization,
342 transformation and transport at the seasonal and synoptic time scales. However, we acknowledge
343 that the temporal coverage of the remote sensing data is restricted to spring and summer. Because of
344 clouds and sea ice, we miss the winter season when tDOC is the most labile (e.g. Wickland et al.,
345 2012) and likely subject to remineralization. In the Mackenzie River, about 25 % of the annual load
346 of labile tDOC occurs during winter (Wickland et al., 2012). Despite this limitation, and in regard to
347 the model-satellite data comparison, the assimilation of remotely sensed tDOC data into Arctic
348 models could still offer an interesting perspective as it might result in more realistic simulated fields
349 of tDOC in spring and summer when the river discharge and tDOC export is the highest. Physical
350 and biological data have already been assimilated into Arctic predictive models to make the
351 simulated sea surface temperature, salinity, sea ice extent and thickness, and chlorophyll more
352 reliable (Simon et al., 2015; Massonnet et al., 2015). We may hence expect the assimilation of
353 remotely sensed tDOC concentrations to mitigate, at least partly, the issues linked to setting up
354 realistic tDOC forcings within predictive models. For instance, the assimilation of remotely sensed
355 tDOC data in open waters might help accounting for the interannual variations of tDOC delivered
356 by rivers, which are not resolved by the coupled model that is constrained by a monthly climatology
357 of tDOC load (see Manizza et al., 2009).
358 Improving the capability of Arctic models to resolve the fate and pathways of tDOC in the AO will
359 require certain limitations to be unlocked. To this purpose, future model developments must lie on
360 the always increasing observational effort realized by mean of field campaigns and new remote
361 sensing techniques. Observations must be used to improve the riverine forcings in order to better
362 encompass the seasonal to interannual variability of the terrigenous dissolved organic matter
363 exported to the coastal AO. Bacterioplankton dynamics also must be better represented in

biogeochemical models. In particular, the processes related to the competition for resources such as dissolved organic carbon and nitrogen of both allochtonous and autochtonous origin are likely to play an important role in mediating bacterioplankton growth and tDOC remineralization in Arctic coastal waters impacted by river plumes. Realistic fields of tDOC simulated by Arctic ocean-biogeochemical coupled models would be helpful for a more accurate assessment of CO_2 fluxes at the ocean-atmosphere interface. Arctic models that would combine realistic terrestrial fluxes of organic matter along with a robust representation of the pathways and processes responsible for its transformation in the AO would open an interesting perspective to address the effect on the Arctic carbon cycle of ongoing and future changes in the land-ocean continuum. The increase in seawater temperature of the AO due to global warming (Timmermans, 2016) might promote in the future the metabolism and respiration rates of marine bacterioplankton (Vaquer-Sunyer et al., 2010; Kritzberg et al., 2010). This enhanced microbial activity could then liberate extra nutrients provided by the remineralization of terrigenous organic matter that will then be available for primary production. This process might have an impact not only on the seasonal cycle of PP in the AO but also implications for the higher levels of the marine food webs of the AO, both benthic and pelagic.

Data availability

Data used in this study are available at http://www.obs-lienss.cnrs.fr/Publications/BGD_data_nc.tar.

Acknowledgments

This research was funded by the Centre national d'études spatiales (CNES) grant #131425-BC T23 to VLF and the Japan Aerospace Exploration Agency (JAXA) GCOM-C project through grant #16RSTK-007867 to AM. We thank a joint contribution to the research programs of UMI Takuvik (CNRS & Université Laval), ArcticNet (Network Centres of Excellence of Canada) and the Canada Excellence Research Chair in Remote Sensing of Canada's New Arctic Frontier (MB). We thank

390 Dimitris Menemenlis and the Estimation of Circulation and Climate of the Ocean (ECCO) group
391 from MIT for providing the physical model we used in this study. We also thank Cécilia Pignon-
392 Mussaud (LIENSs) for her help in processing the figure 1.
393

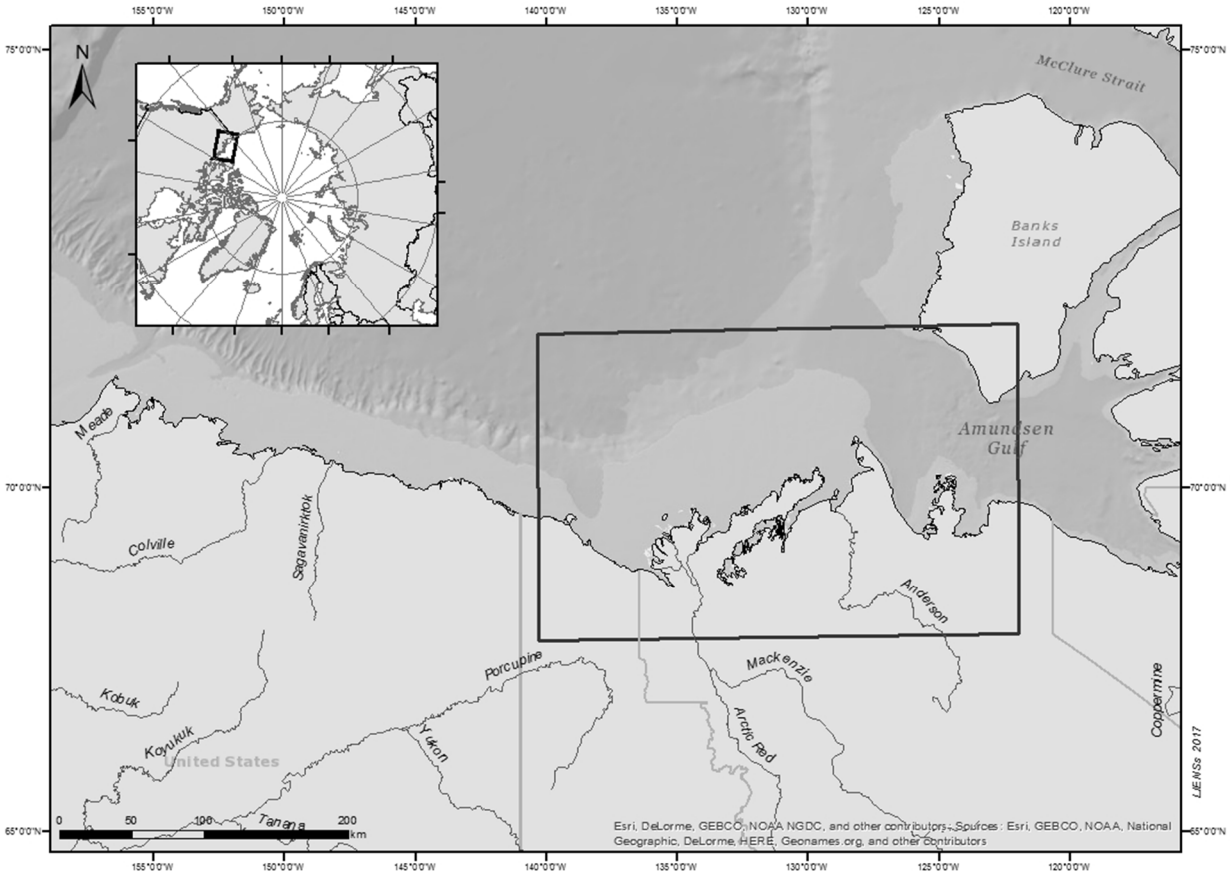

394

395 **Figure 1.** Map of the Canadian Beaufort Sea. The location of the study area is outlined with a

396 rectangle.

397

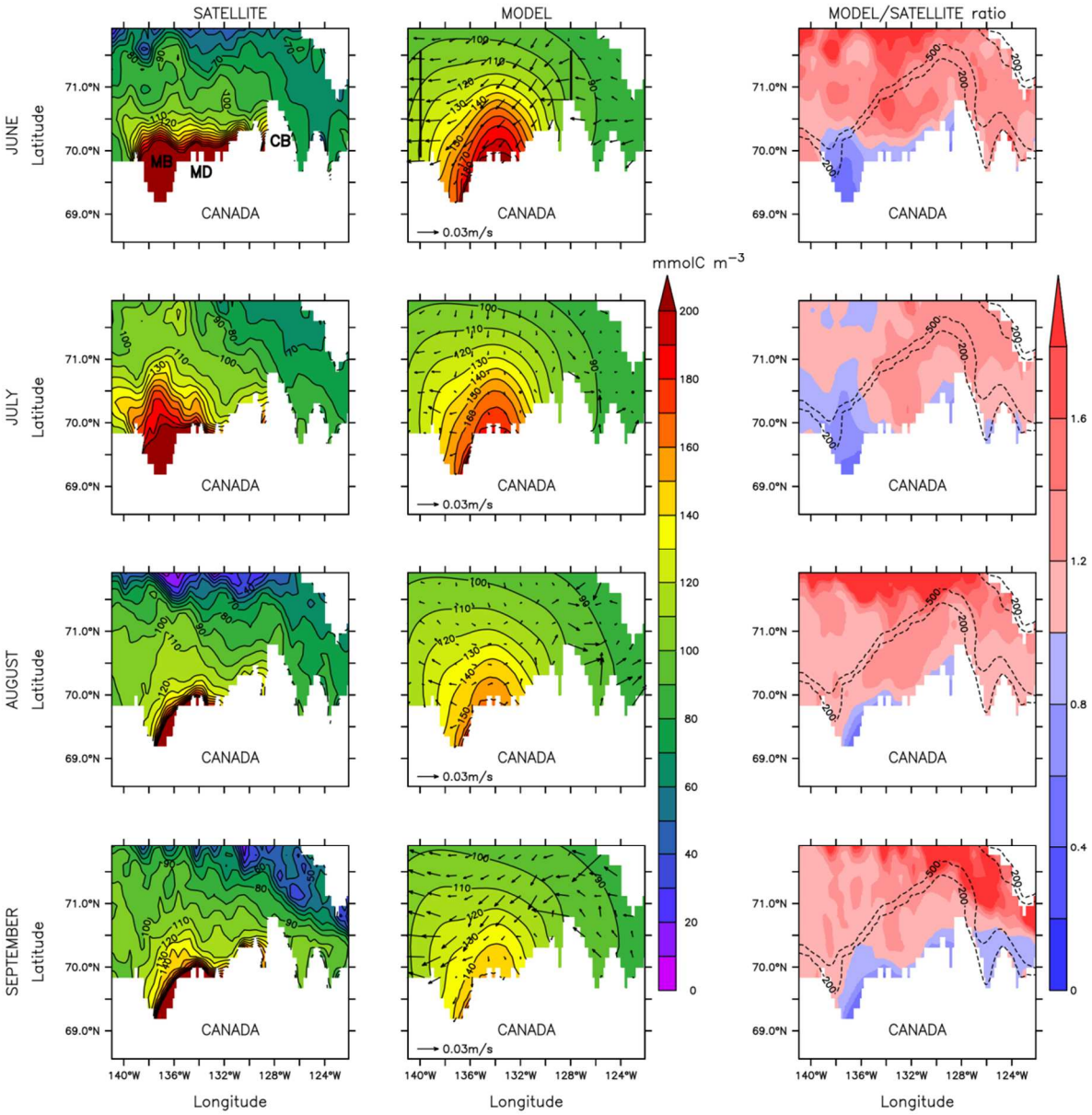

Figure 2. Monthly climatology (2003-2011) of surface tDOC concentration (mmolC m^{-3}) in the Beaufort Sea estimated from remotely sensed ocean color data (left panels) and by the biogeochemical model (middle panels) for June, July, August and September. The Mackenzie Bay (MB), Mackenzie delta (MD) and Cape Bathurst (CB) cited in the text are shown on the upper left panel. The isolines of tDOC concentration are overlaid (black full lines). In the middle panels, simulated surface currents (m s^{-1}) are overlaid. The two straight lines in the upper-middle panel refer to transects along which surface tDOC fluxes were computed. The right panels show the model over satellite tDOC data ratio with the 200 m and 500 m isobaths overlaid.

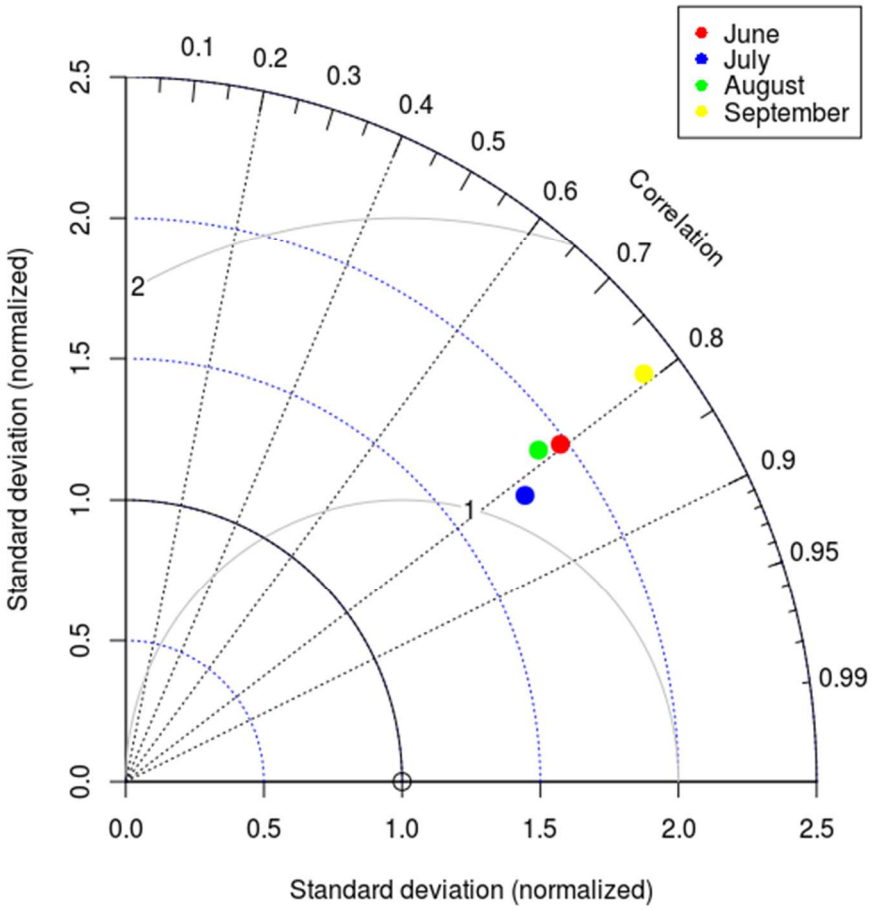

407

408 **Figure 3.** Taylor diagram displaying a statistical comparison between the simulated and remotely
409 sensed tDOC concentrations. The x-axis and y-axis show the model standard deviation relative to
410 the satellite standard deviation. The open circle on the x-axis represents the reference point. The
411 model-satellite correlation is represented in polar coordinates (angle from the x-axis). The light grey
412 full lines indicate the RMSE relative to the satellite standard deviation.

413

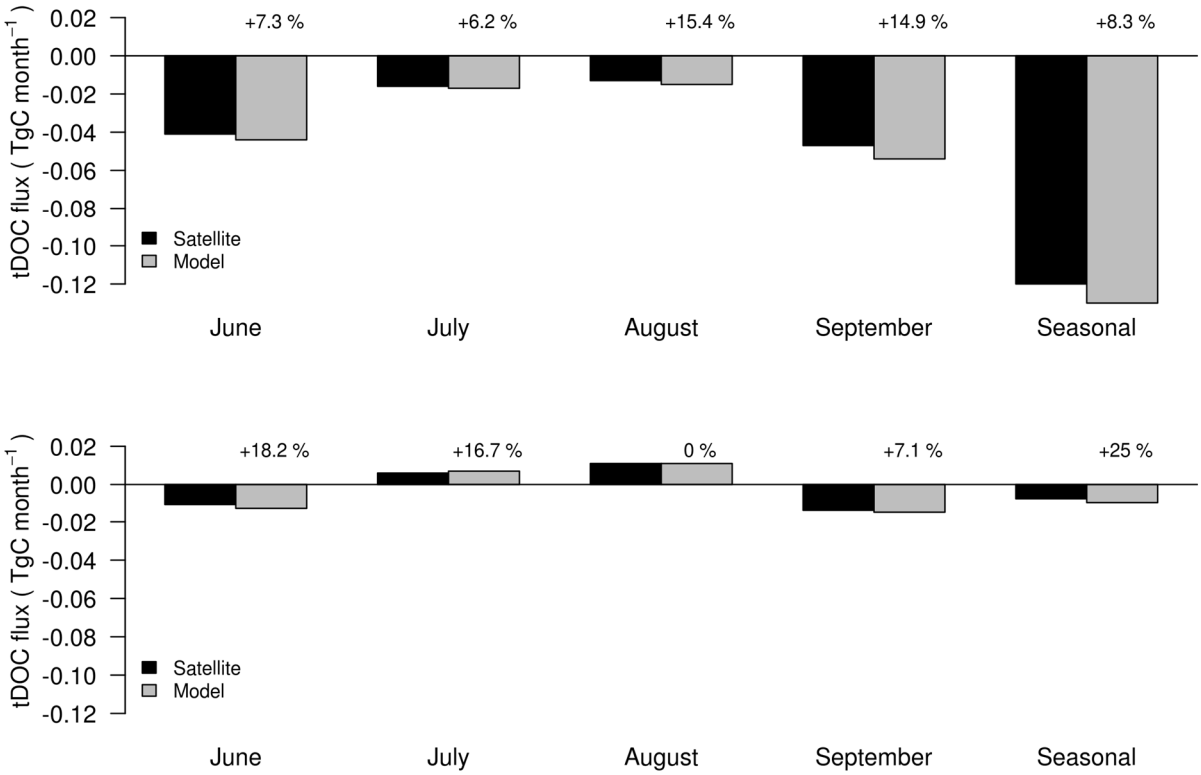

414

415 **Figure 4.** Monthly flux of surface tDOC (TgC month^{-1}) computed along transects located west of
416 the Mackenzie Trough (139°W ; 69.5°N-71°N) (upper panel) and at Cape Bathurst (128°W ;
417 69.5°N-71°N) (lower panel). Transects are shown in figure 1 in the upper-middle panel. Negative
418 values indicate a westward flux. Percentages refer to the model data relative to the satellite data.
419 The seasonal flux refers to the 4-month net flux.

420

421 **Table 1.** Skill metrics of comparison computed based on the 2003-2011 monthly climatologies of

422 tDOC.

423

Metric	June	July	August	September
Correlation coefficient	0.79	0.82	0.78	0.79
Unbiased RMSE (mmolC m^{-3})	41.4	29.4	26.0	29.3
Model efficiency	0.49	0.60	0.26	0.38
Geometric statistics using log-transformed data				
Model bias	1.24	1.07	1.32	1.21
RMSE	1.07	1.02	1.12	1.06

424

425

426 **Table 2.** Areal stock (TgC) of sea surface tDOC computed over the Mackenzie shelf (delimited by
427 the 300 m isobaths) from the model and satellite data. The bias (%) refers to the model data relative
428 to the satellite data. The seasonal areal stock refers to the 4-month average ± standard deviation.

	June	July	August	September	Seasonal
Model	1.48	1.40	1.32	1.28	1.37±0.07
Satellite	1.51	1.44	1.22	1.30	1.37±0.11
Bias	-2	-2.8	+8.2	-1.5	0

429

430

References

Aagaard, K. and Carmack, E. C.: The role of sea ice and other fresh water in the Arctic circulation, J. Geophys. Res., 94, doi:10.1029/JC094iC10p14485. Issn: 0148-0227, 1989.

Abbott, B. W., Jones, J. B., Schuur, E. A. G., Chapin, F. S., III, Bowden, W. B., Bret-Harte, M. S., et al.: Biomass offsets little or none of permafrost carbon release from soils, streams, and wildfire: an expert assessment, Environmental Discussion paper Research Letters, 11(3), 034014–14, doi:10.1088/1748-9326/11/3/034014, 2016.

Alling, V., Sanchez-Garcia, L., Porcelli, D., Pugach, S. , Vonk, J. E., van Dongen, B., Mörth, C.-M., Anderson, L. G., Sokolov, A., Andersson, P., Humborg, C., Semiletov, I., and Gustafsson, Ö.: Nonconservative behavior of dissolved organic carbon across the Laptev and East Siberian seas, Global Biogeochem. Cy., 24, GB4033, doi:10.1029/2010GB003834, 2010.

Bélanger, S., Xie, H., Krotkov, N., Larouche, P., Vincent, W. F., and Babin, M.: Photomineralization of terrigenous dissolved organic matter in Arctic coastal waters from 1979 to 2003: Interannual variability and implications of climate change, Global Biogeochem. Cy., 20, GB4005, doi:10.1029/2006GB002708, 2006.

Bélanger S., Babin, M., and Tremblay, J.-E.: Increasing cloudiness in Arctic damps the increase in phytoplankton primary production due to sea ice receding, Biogeosciences, 10, 4087–4101, doi:10.5194/bg-10-4087-2013, 2013.

Bell, L. E., Bluhm, B. A., and Iken, K.: Influence of terrestrial organic matter in marine food webs of the Beaufort Sea shelf and slope, Mar. Ecolo. Prog. Ser., 550, 1–24, doi:10.3354/meps11725, 2016.

Bring, A., Fedorova, I., Dibike, Y., Hinzman, L., Mård, J., Mernild, S. H., Prowse, T., Semenova, O., Stuefer, S. L., and Woo M.-K.: Arctic terrestrial hydrology: A synthesis of processes,

454 regional effects, and research challenges, J. Geophys. Res. Biogeosci., 121, 621–649,
455 doi:10.1002/2015JG003131, 2016.

456 Buesseler K. O.: The decoupling of production and particulate export in the surface ocean, Global
457 Biogeochem. Cy., 12, 297–310, 1998.

458 Condron, A., Winsor, P., Hill, C. N., and Menemenlis, D.: Response of Arctic freshwater budget to
459 extreme NAO forcing, J. Clim., 22, 2422–2437, 2009.

460 Davies, K. F.: Mackenzie River input to the Beaufort Sea, Beaufort Sea Project, Technical Report
461 15, Institute of Ocean Sciences, Sidney, British, Columbia, 72 p, 1975.

462 Dittmar, T., and Kattner, G.: The biogeochemistry of the river and shelf ecosystem of the Arctic
463 Ocean: a review, Mar. Chem., 83, 103–120, doi:10.1016/S0304-4203(03)00105-1, 2003.

464 Doney, S.C., Lima, I., Moore, J. K., and Takahashi, T.: Skill metrics for confronting global upper
465 ocean ecosytem-biogeochemistry models against field and remote sensing data, J. Mar. Syst.,
466 76, 95–112, doi:10.1016/j.jmarsys.2008.05.015, 2009.

467 Doxaran, D., Devred, E., and Babin, M.: A 50 % increase in the mass of terrestrial particles
468 delivered by the Mackenzie River into the Beaufort Sea (Canadian Arctic Ocean) over the last
469 10 years, Biogeosci., 12, 3551–3565, doi:10.5194/bg-12-3551-2015, 2015.

470 Dunton, K. H., Weingartner, T., and Carmack, E. C.: The nearshore western Beaufort Sea
471 ecosystem: circulation and importance of terrestrial carbon in arctic coastal food webs, Progr.
472 Oceanogr., 71, 362–378, doi:10.1016/j.pocean.2006.09.011, 2006.

473 Emmerton, C. A., Lesack, L. F. W., and Vincent, W. F.: Nutrient and organic matter patterns across
474 the Mackenzie River, estuary and shelf during the seasonal recession of sea-ice, J. Marine Syst.,
475 74, 741–755, doi:10.1016/j.jmarsys.2007.10.001, 2008.

476 Griffin, C. G., Frey, K. E., Rogan, J., and Holmes, R. M.: Spatial and interannual variability of
477 dissolved organic matter in the Kolyma River, East Siberia, observed using satellite imagery, J.
478 Geophys. Res., 116, G03018, doi:10.1029/2010JG001634, 2011.

479 Haine, T. W. N., Curry, B., Gerdes, R., Hansen, E., Karcher, M., Lee, C., Rudels, B., Spreen, G., de
480 Steur, L., Stewart, K. D., and Woodgate R.: Arctic freshwater export: Status, mechanisms, and
481 prospects, Global and Planetary Change, 125, 13–35,doi:/10.1016/j.gloplacha.2014.11.013,
482 2015.

483 Herrault, P.-A., Gandois, L., Gascoin, S., Tananaev, N., Le Dantec, T., and Teisserenc, R.: Using
484 high spatio-temporal optical remote sensing to monitor dissolved organic carbon in the Arctic
485 river Yenisei, Remote Sens., 8, 803, doi:10.3390/rs8100803, 2016.

486 Holmes, R. M., McClelland, J. W., Raymond, P. A., Frazer, B. B., Peterson, B. J., and Stieglitz, M.:
487 Lability of DOC transported by Alaskan rivers to the Arctic Ocean, Geophys. Res. Lett., 35,
488 L03402. doi:10.1029/2007GL032837, 2008.

489 Holmes, R. M., McClelland, J. W., Peterson, B. J., Tank, S. E., Bulygina, E., Eglinton, T. I.,
490 Gordeev, V. V., Gurtovaya, T. Y., Raymond, P. A., Repeta, D. J., Staples, R., Striegl, R. G.,
491 Zhulidov, A. V., and Zimov, S. A.: Seasonal and annual fluxes of nutrients and organic matter
492 from large rivers to the Arctic Ocean and surrounding seas, Estuar. Coasts, 35, 369–382,
493 doi:10.1007/s12237-011-9386-6, 2012.

494 Holmes, R. M., Shiklomanov, A. I., Tank, S. E., McClelland, J. W., and Tretiakov, M.: River
495 discharge, Arctic Report Card: Update for 2015, http://www.arctic.noaa.gov/Report-
496 Card/Report-Card-2015/ArtMID/5037/ArticleID/227/River-Discharge, 2015.

497 Kicklighter, D. W., Hayes, D. J., MacClelland, J. W., Peterson, B. J., McGuire, A. D., and Melillo,
498 J. M.: Insights and issues with simulating terrestrial DOC loading of Arctic river networks,
499 Ecol. App., 23, 1817–1836, doi:10.1890/11-1050.1, 2013.

500 Kritzberg, E., Duarte, C. M., and Wassmann, P.: Changes in Arctic marine bacterial carbon
501 metabolism in response to increasing temperature, Polar Biol., 33, 1673–1682,
502 doi:10.1007/s00300-010-0799-7, 2010.

503 Lammers, R. B., Shiklomanov, A. I., Vörösmarty, C. J., Fekete, B. M., and Peterson, B. J.:
504 Assessment of contemporary Arctic river runoff based on observational discharge records, J.
505 Geophys. Res., 106(D4), 3321–3334, doi:10.1029/2000JD900444, 2001.

506 Lee, Y. J., Matrai, P. A., Friedrichs, M. A. M., Saba, V. S., Aumont, O., Babin, M., Buitenhuis, E.
507 T., Chevallier, M., de Mora, L., Dessert, M., Dunne, J. P., Ellingsen, I., Feldman, D., Frouin, R.,
508 Gehlen, M., Gorgues, T., Ilyina, T., Jin, M., John, J. G., Lawrence, J., Manizza, M., Menkes, C.
509 E., Perruche, C., Le Fouest, V., Popova, E., Romanou, A., Samuelsen, A., Schwinger, J.,
510 Séférian, R., Stock, C. A., Tjiputra, J., Tremblay, B. L., Ueyoshi, K., Vichi, M., Yool, A., and
511 Zhang, J.: Net primary productivity estimates and environmental variables in the Arctic Ocean:
512 An assessment of coupled physical-biogeochemical models, J. Geophys. Res.,
513 doi:10.1002/2016JC011993, 2016.

514 Le Fouest V., Babin, M., and Tremblay, J.-E.: The fate of riverine nutrients on Arctic shelves,
515 Biogeosciences, 10, 3661–3677, doi:10.5194/bg-10-3661-2013, 2013.

516 Le Fouest, V., Manizza, M., Tremblay, B., and Babin, M.: Modeling the impact of riverine DON
517 removal by marine bacterioplankton on primary production in the Arctic Ocean,
518 Biogeosciences, 12, 3385–3402, doi:10.5194/bg-12-3385-2015, 2015.

519 Letscher, R. T., Hansell, D. A., and Kadko, D.: Rapid removal of terrigenous dissolved organic
520 carbon over the Eurasian shelves of the Arctic Ocean, Mar. Chem., 123, 78–87,
521 doi:10.1016/j.marchem.2010.10.002, 2011.

522 Losch, M., Menemenlis, D., Campin, J.-M., Heimbach, P., and Hill, C.: On the formulation of sea-
523 ice models. Part 1: Effects of different solver implementations and parameterizations, Ocean
524 Model., 33, 129–144, doi:10.1016/j.ocemod.2009.12.008, 2010.

McClelland, J. W., Holmes, R. M., Dunton, K. H., and Macdonald, R. W.: The Arctic Ocean estuary, Estuar. Coast., 35, 353–368,doi:10.1007/s12237-010-9357-3, 2012.

McGuire A. D., Anderson, L. G., Christensen, T. R., Dallimore, S., Guo, L., Hayes, D. J., Heimann, M., Lorenson, T. D., Macdonald, R.W., and Roulet, N.: Sensitivity of the carbon cycle in the Arctic to climate change, Ecol. Monogr., 79, 523–555, doi:10.1890/08-2025.1, 2009.

Macdonald, R. W., Paton, D. W., Carmack, E. C., and Omstedt, A.: The freshwater budget and under-ice spreading of Mackenzie River water in the Canadian Beaufort Sea based on salinity and 18 O / 16 O measurements in water and ice, J. Geophys. Res., 100, 895–919, 1995, 1995.

Manizza, M., Follows, M. J., Dutkiewicz, S., McClelland, J. W., Menemenlis, D., Hill, C. N., Townsend-Small, A., and Peterson, B. J.: Modeling transport and fate of riverine dissolved organic carbon in the Arctic Ocean, Global Biogeochem. Cy., 23, GB4006, doi:10.1029/2008GB003396, 2009.

Manizza, M., Follows, M., Dutkiewicz, S., Menemenlis, D., McClelland, J. W., Hill, C. N., Peterson, B. J., and Key, R. M.: A model of the Arctic Ocean carbon cycle, J. Geophys. Res., 116(C12), C12020, doi:10.1029/2011JC006998, 2011.

Manizza, M., Follows, M. J., Dutkiewicz, S., Menemenlis, D., Hill, C. N., and Key, R. M.: Changes in the Arctic Ocean CO_2 sink (1996–2007): A regional model analysis, Global Biogeochem. Cy., 27, 1108–1118, doi:10.1002/2012GB004491, 2013.

Mann, P. J., Davydova, A., Zimov, N., Spencer, R. G. M., Davydov, S., Bulygina, E., Zimov, S., and Holmes, R. M.: DOM composition and lability during the Arctic spring freshet on the River Kolyma, Northeast Siberia, J. Geophys. Res., 117, G01028, doi:10.1029/2011JG001798, 2012.

Mann, P. J., Spencer, R. G. M., Hernes, P. J., Six, J., Aiken, G. R., Tank, S. E., McClelland, J. W., Butler, K .D., Dyda, R. Y., and Holmes, R. M.: Pan-Arctic Trends in Terrestrial Dissolved

549 Organic Matter from Optical Measurements, Front. Earth Sci., 4, 25, 10.3389/feart.2016.00025,
550 2016.

551 Massonnet, F., Fichefet, T., and Goosse, H.: Prospects for improved seasonal Arctic sea ice
552 predictions from multivariate data assimilation, Ocean Model., 88, 16–25,
553 doi:10.1016/j.ocemod.2014.12.013, 2015.

554 Matsuoka, A., Hill, V., Huot, Y., Babin, M., and Bricaud, A.: Seasonal variability in the light
555 absorption properties of Western Arctic waters: parameterization of the individual components
556 of absorption for ocean color applications, J. Geophys. Res., 116, C02007,
557 doi:10.1029/2009JC005594, 2011.

558 Matsuoka, A., Bricaud, A., Benner, R., Para, J., Sempéré, R., Prieur, L., Bélanger, S., and Babin, M.:
559 Tracing the transport of colored dissolved organic matter in water masses of the Southern
560 Beaufort Sea: relationship with hydrographic characteristics, Biogeosciences, 9, 925–940,
561 doi :10.5194/bg-9-925-2012, 2012.

562 Matsuoka, A., Hooker, S. B., Bricaud, A., Gentili, B., and Babin, M.: Estimating absorption
563 coefficients of colored dissolved organic matter (CDOM) using a semi-analytical algorithm for
564 southern Beaufort Sea waters : application to deriving concentrations of dissolved organic
565 carbon from space, Biogeosci., 10, 917–927, doi :10.5194/bg-10-917-2013, 2013.

566 Matsuoka, A., Babin, M., Doxaran, D., Hooker, S. B., Mitchell, B. G., Bélanger, S., and Bricaud, A.:
567 A synthesis of light absorption properties of the Pan-Arctic Ocean: application to semi-
568 analytical estimates of dissolved organic carbon concentrations from space, Biogeosci., 11,
569 3131–3147, doi:10.5194/bg-11-3131-2014, 2014.

570 Matsuoka, A., Babin, M., and Devred, E. C.: A new algorithm for discriminating water sources
571 from space: a case study for the southern Beaufort Sea using MODIS ocean color and SMOS
572 salinity data, Remote Sens. Env., 184, 124–138, http://dx.doi.org/10.1016/j.rse.2016.05.006,
573 2016.

574 Matsuoka, A., Boss, E., Babin, M., Karp-Boss, L., Hafez, M., Chekalyuk, A., Proctor, C. W.,
575 Werdell, P. J., and Bricaud, A.: Pan-Arctic optical characteristics of colored dissolved organic
576 matter: Tracing dissolved organic carbon in changing Arctic waters using satellite ocean color
577 data, Remote Sens. Env., 200, 89–101, doi:10.1016/j.rse.2017.08.009, 2017.

578 Menemenlis, D., Hill, C., Adcroft, A., Campin, J.-M., Cheng, B., Ciotti, B., Fukumori, I., Heimbach,
579 P., Henze, C., Kohl, A., Lee, T., Stammer, D., Taft, J., and Zhang, J.: NASA supercomputer
580 improves prospects for ocean climate research, Eos Trans. AGU, 86, 89–96, 2005.

581 Mulligan, R. P., Perrie, W., and Solomon, S.: Dynamics of the Mackenzie River plume on the inner
582 Beaufort shelf during an open water period in summer, Estuar. Coast Shelf Sci., 89, 214–220,
583 doi:10.1016/j.ecss.2010.06.010, 2010.

584 Nash, J., and Sutcliffe, J.: River flow forecasting through conceptual models, part 1 – a discussion
585 of principles, J. Hydrol., 10, 282–290, 1970.

586 Nguyen, A. T., Menemenlis, D., and Kwok, R.: Improved modeling of the Arctic halocline with a
587 subgrid-scale brine rejection parameterization, J. Geophys. Res., 114, C11014,
588 doi:10.1029/2008JC005121, 2009.

589 Nguyen, A. T., Menemenlis, D., and Kwok, R.: Arctic ice-ocean simulation with optimized model
590 parameters: Approach and assessment, J. Geophys. Res., 116(C4), C04025,
591 doi:10.1029/2010JC006573, 2011.

592 Onogi, K., Tsutsui, J., Koide, H., Sakamoto, M., Kobayashi, S., Hatsushika, H., Matsumoto, T.,
593 Yamazaki, N., Kamahori, H., Takahashi, K., Kadokura, S., Wada, K., Kato, K., Oyama, R.,
594 Ose, T., Mannoji, N., and Taira, R.: The JRA-25 Reanalysis, J. Meteor. Soc. Japan, 85, 369–
595 432, doi:10.2151/jmsj.85.369, 2007.

596 Opsahl, S., Benner, R., and Amon, R. M.: Major flux of terrigenous dissolved organic matter
597 through the Arctic Ocean, Limnol. Oceanogr., 44, 2017–2023, doi:10.4319/lo.1999.44.8.2017,
598 1999.

599 Ortega-Retuerta, E., Jeffrey, W. F., Babin, M., Bélanger, S., Benner, R., Marie, D., Matsuoka, A.,
600 Raimbault, P., and Joux, F.: Carbon fluxes in the Canadian Arctic: patterns and drivers of
601 bacterial abundance, production and respiration on the Beaufort Sea margin, Biogeosciences, 9,
602 3679–3692, doi:10.5194/bg-9-3679-2012, 2012.

603 Osburn, C. L., Retamal, L., and Vincent, W. F.: Photoreactivity of chromophoric dissolved organic
604 matter transported by the Mackenzie River to the Beaufort Sea, Mar. Chem., 115,
605 doi:10.1016/j.marchem.2009.05.003, 2009.

606 Para, J., Charrière, B., Matsuoka, A., Miller, W. L., Rontani, J. F., and Sempéré, R.: UV/PAR
607 radiation and DOM properties in surface coastal waters of the Canadian shelf of the Beaufort
608 Sea during summer 2009, Biogeosciences, 10, 2761-2774, doi:10.5194/bg-10-2761-2013, 2013.

609 Ping, C.-L., Michaelson, G. J., Guo, L., Torre Jorgenson, M., Kanevskiy, M., Shur, Y., Dou, F., and
610 Liang, J.: Soil carbon and material fluxes across the eroding Alaska Beaufort Sea coastline, J.
611 Geophys. Res., 116, G02004, doi:10.1029/2010JG001588, 2011.

612 Rachold, V., Eiken, H., Gordeev, V. V., Grigoriev, M. N., Hubberten, H.-W., Lisitzin, A. P.,
613 Shevchenko, V. P., and Schirmeister, L.: Modern terrigenous organic carbon input to the Arctic
614 Ocean, in The Organic Carbon Cycle in the Arctic Ocean, edited by R. S. Stein and R. W.
615 Macdonald, 33–55, Springer, New York, 2004.

616 Rawlins, M. A., Steele, M., Holland, M., Adam, J., Cherry, J., Francis, J., Groisman, P., Hinzman,
617 L., Huntington, T., Kane, D., Kimball, J., Kwok, R., Lammers, R., Lee, C., Lettenmaier, D.,
618 McDonald, K., Podest, E., Pundsack, J., Rudels, B., Serreze, M., Shiklomanov, A., Skagseth,
619 O., Troy, T., Vorosmarty, C., Wensnahan, M., Wood, E., Woodgate, R., Yang, D., Zhang, K.,
620 and Zhang, T.: Analysis of the Arctic System for Freshwater Cycle Intensification:
621 Observations and Expectations, J. Climate, 23, 5715–5737, doi:10.1175/2010JCLI3421.1, 2010.

622 Raymond, P. A., McClelland, J. W., Holmes, R. M., Zhulidov, A. V., Mull, K., Peterson, B. J.,
623 Striegl, R. G., Aiken, G. R., and Gurtovaya, T. Y.: Flux and age of dissolved organic carbon

624 exported to the Arctic Ocean: A carbon isotopic study of the five largest arctic rivers, Global
625 Biogeochem. Cy., 21, GB4011, doi:10.1029/2007GB002934, 2007.

626 Romanovsky, V. E., Drozdov, D. S., Oberman , N. G., Malkova, G. V., Kholodov, A. L.,
627 Marchenko, S. S., Moskalenko, N. G., Sergeev, D. O., Ukraintseva, N. G., Abramov, A. A.,
628 Gilichinsky, D. A., and Vasiliev, A. A.: Thermal State of Permafrost in Russia, Permafrost and
629 Periglacial Process., 21, 136–155. doi:10.1002/ppp.683, 2010.

630 Semiletov, I., Pipko, I., Gustafsson, Ö., Anderson, L. G., Sergienko, V., Pugach, S., Dudarev, O.,
631 Charkin, A., Gukov, A., Bröder, L., Andersson, A., Spivak, E., and Shakhova, N.: Acidification
632 of East Siberian Arctic Shelf waters through addition of freshwater and terrestrial carbon,
633 Nature Geosci., 9, 361–365, doi:10.1038/ngeo2695, 2016.

634 Serreze, M., Barret, A. P., Slater, A. G., Woodgate, R. A., Aagard, K., Lammers, R. B., Steele, M.,
635 Mortitz, R., Meredith, M., and Lee, C. M.: The large-scale fresh water cycle of the Arctic, J.
636 Geophys. Res., 111, C11010, doi:10.1029/2005JC003424, 2006.

637 Shiklomanov, I., Shiklomanov, A., Lammers, R., Peterson, B., and Vorosmarty, C.: The dynamics
638 of river water inflow to the Arctic Ocean, in The Freshwater Budget of the Arctic Ocean, edited
639 by E. Lewis, 281–296, Kluwer Acad., Boston, Mass, 2000.

640 Simon, E., Samuelsen, A., Bertino, L., and Mouysset, S.: Experiences in multiyear combined state-
641 parameter estimation with an ecosystem model of the North Atlantic and Arctic Oceans using
642 the Ensemble Kalman Filter, J. Mar. Syst., 152, 1–17, doi:10.1016/j.jmarsys.2015.07.004.

643 Stein, R., and Macdonald, R. W.: The Organic Carbon Cycle in the Arctic Ocean, Springer,
644 Heidelberg, Germany, 2015.

645 Stow, A. C., Jolliff, J., McGillicuddy Jr., D. J., Doney, S. C., Allen, J. I., Friedrichs, M. A. M., Rose,
646 K. A., and Wallhead, P.: Skill Assessment for coupled biological/physical models of marine
647 systems, J. Mar. Syst., 76, 4–15, doi:10.1016/j.jmarsys.2008.03.011, 2009.

Striegl, R. G., Aiken, G. R., Dornblaser, M. M., Raymond, P. A., and Wickland, K. P.: A decrease in discharge-normalized DOC export by the Yukon River during summer through autumn, Geophysical Research Letters, 32(21), L21413, doi:10.1029/2005GL024413, 2005.

Tank, S. E., Manizza, M., Holmes, R. M., McClelland, J. W., and Peterson, B. J.: The Processing and Impact of Dissolved Riverine Nitrogen in the Arctic Ocean, Estuar. Coasts, 35, doi:10.1007/s12237-011-9417-3, 2012.

Tank, S. E., Striegl, R. G., McClelland, J. W., and Kokelj, S. V: Multi-decadal increases in dissolved organic carbon and alkalinity flux from the Mackenzie drainage basin to the Arctic Ocean, Environ. Res. Lett., 11, 054015, doi:10.1088/1748-9326/11/5/054015, 2016.

Tanski, G., Couture, N., Lantuit, H., Eulenburg, A., and Fritz, M.: Eroding permafrost coasts release low amount of dissolved organic carbon from ground ice into the nearshore zone of the Arctic Ocean, Global Biogeochem. Cy., 30, 1054–1068, doi:10.1002/2015GB005337, 2016.

Tarnocai, C., Canadell, J. G., Schuur, E. A. G., Kuhry, P., Mazhitova, G., and Zimov, S.: Soil organic carbon pools in the northern circumpolar permafrost region, Global Biogeochem. Cy., 23, GB2023, doi:10.1029/2008gb003327, 2009.

Taylor, K. E.: Summarizing multiple aspects of model performance in a single diagram, J. Geophys. Res.,106, 7183–7192, 2001.

Timmermans, M.-L.: Sea Surface Temperature, Arctic Report Card: Update for 2016, http://www.arctic.noaa.gov/Report-Card/Report-Card-2016/ArtMID/5022/ArticleID/285/Sea-Surface-Temperature, 2016.

Vallières, C., Retamal, L., Osburn, C., and Vincent, W. F.: Bacterial production and microbial food web structure in a large Arctic river and the coastal Arctic Ocean, J. Mar. Syst., 74, 756–773, doi:10.1016/j.jmarsys.2007.12.002, 2008.

671 Vaquer-Sunyer, R., Duarte, C. M., Santiago, E., Wassmann, P., and Reigstad, M.: Experimental
672 evaluation of planktonic respiration response to warming in the European Arctic sector, Polar
673 Biol., 33, 1661–1671, doi:10.1007/s00300-010-0788-x, 2010.

674 Vihma, T., Screen, J., Tjernström, M., Newton, B., Zhang, X., Popova, V., Deser, C., Holland, M.,
675 and Prowse, T.: The atmospheric role in the Arctic water cycle: A review on processes, past
676 and future changes, and their impacts, J. Geophys. Res. Biogeosci., 121, 586–620,
677 doi:10.1002/2015JG003132, 2016.

678 Wang, M. and Shi, W.: The NIR-SWIR combined atmospheric correction approach for MODIS
679 ocean color data processing, Opt. Express, 15, 15722–15722, 2007.

680 Wickland, K. P., Aiken, G. R., Butler, K., Dornblaser, M. M., Spencer, R. G. M., and Striegl, R. G.:
681 Biodegradability of dissolved organic carbon in the Yukon River and its tributaries: Seasonality
682 and importance of inorganic nitrogen, Global Biogeochem. Cy., 26, GB0E03,
683 doi:10.1029/2012GB004342, 2012.

684 Yang, D., Shi, X., and Marsh, P.: Variability and extreme of Mackenzie River daily discharge
685 during 1973-2011, Quatern. Internat., 380–381, 159–168, doi:10.1016/j.quaint.2014.09.023,
686 2015.